The spectral phasor approach to resolving membrane order with environmentally sensitive dyes

Agustín Mangiarotti* **and Rumiana Dimova***
Max Planck Institute of Colloids and Interfaces, Science Park Golm, Potsdam, Germany
*Corresponding authors. e-mail address: Mangiarotti@mpikg.mpg.de; Dimova@mpikg.mpg.de

Contents

Abstract

Hyperspectral imaging is a technique that captures a three-dimensional array of spectral information at each spatial location within a sample, enabling precise characterization and discrimination of biological structures, materials, and chemicals, based on their unique spectral features. Nowadays most commercially available confocal microscopes allow hyperspectral imaging measurements, providing a valuable source of spatially resolved spectroscopic data. Spectral phasor analysis quantitatively and graphically transforms the fluorescence spectra at each pixel of a hyperspectral image into points in a polar plot, offering a visual representation of the spectral characteristics of fluorophores within the sample. Combining the use of

Methods in Enzymology
ISSN 0076-6879, https://doi.org/10.1016/bs.mie.2024.01.024
Copyright © 2024 Elsevier Inc. All rights are reserved, including those for text and data mining, AI training, and similar technologies.

environmentally sensitive dyes with phasor analysis of hyperspectral images provides a powerful tool for measuring small changes in lateral membrane heterogeneity. Here, we focus on applications of spectral phasor analysis for the probe LAURDAN on model membranes to resolve packing and hydration. The method is broadly applicable to other dyes and to complex systems such as cell membranes.

1. Introduction

1.1 Nano-environmental probes and LAURDAN spectroscopic properties

Coexisting phases in membranes can be visualized by fluorescence microscopy using lipid-based fluorescent dyes, which generally show different partitioning between the phases, providing contrast for distinguishing micron-sized domains. Some special types of fluorescent dyes, called environment/polarity-sensitive dyes, can provide quantitative information about the phase state of the membrane resolving lateral membrane heterogeneities (Klymchenko, 2023), even if they are below the optical resolution (Sanchez, Tricerri, & Gratton, 2012). These dyes display changes in their spectroscopic properties in response to the physicochemical state of the membrane (Gunther, Malacrida, Jameson, Gratton, & Sánchez, 2021; Klymchenko, 2023). One of the most popular and studied environment sensitive dyes for membranes is 6-dodecanoyl-2-dimethylaminonaphthalene (LAURDAN) originally synthesized by Weber and Farris (1979). LAURDAN is a fluorescent probe that is sensitive to membrane polarity and dipolar relaxation of its environment, and it partitions equally between the gel and disordered phases (Bagatolli, 2013; Gunther et al., 2021). The sensitivity of LAURDAN, reflected in shifts in its emission spectra, is due to the change in dipole moment resulting from an increase in charge separation upon excitation, as shown in Fig. 1. The increase in the dipole moment of the dye molecule induces the relaxation of the solvent dipoles: if the solvent molecules are allowed to reorient during the time in which the probe is in the excited state, the fluorescence emission will be red-shifted (Fig. 1A and B). Conversely, if the dye is in an environment where the dynamics of the solvent molecules are restricted and cannot reorient during the excited state, the spectrum will be blue-shifted. In particular, in membranes, LAURDAN fluorescence is sensitive to the dynamics of a few water molecules located near the glycerol backbone of glycerophospholipids (Bagatolli, 2013), see Fig. 1C. This makes the spectroscopic properties LAURDAN a very

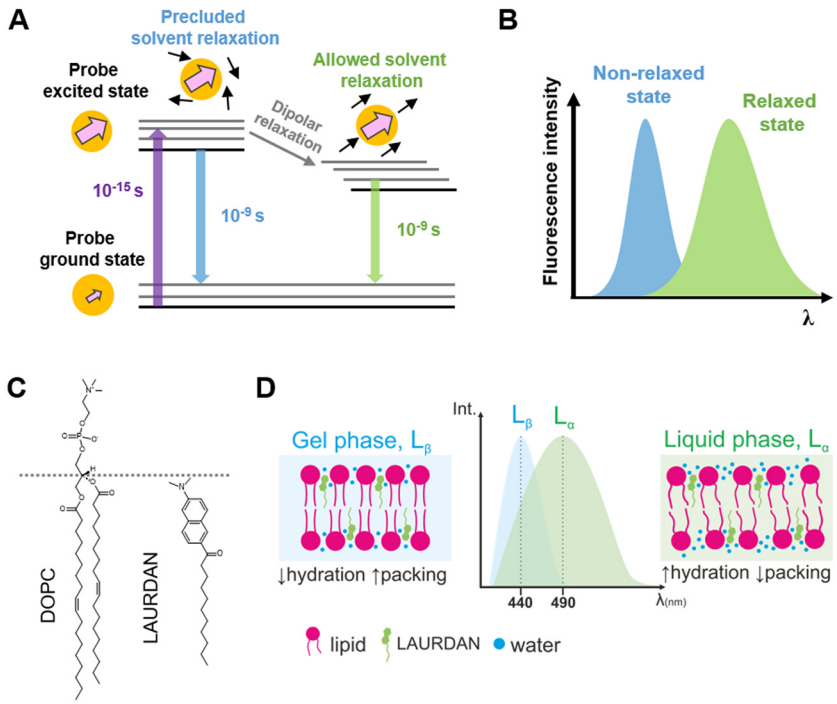

Fig. 1 (A) Perrin-Jablonski diagram showing the phenomenon of solvent dipolar relaxation. Upon excitation, there is an increase in the dipole moment of the probe (pink arrow). When the solvent dipoles (black arrows) are free to reorient and align with the probe in its excited state, the fluorescence emission is red-shifted as a result of the energy reduction, as seen in (B). (C) Molecular structures of DOPC and LAURDAN. The dashed line indicates their approximate positions with respect to the bilayer central plane (~1.5 nm) (Jurkiewicz, Olżyńska, Langner, & Hof, 2006). (D) Scheme illustrating the spectral shifts for LAURDAN in membranes with different properties: highly packed and dehydrated membranes (left), such as those in the gel-phase state (L_β) show a blue-shifted spectrum with a maximum located near 440 nm. Membranes in a liquid phase state (L_α, right) will present a red-shifted spectrum with a maximum centered near 490 nm (Bagatolli, 2013; Gunther et al., 2021). *All panels are adapted from Mangiarotti, A., Siri, M., Tam, N. W., Zhao, Z., Malacrida, L., & Dimova, R. (2023). Biomolecular condensates modulate membrane lipid packing and hydration. Nature Communications, 14(1), 6081.*

suitable tool to address the membrane phase state and hydration level (Bagatolli, 2013; Gunther et al., 2021; Leung, Brewer, Bagatolli, & Thewalt, 2019; Malacrida et al., 2016; Mangiarotti & Bagatolli, 2021).

One of the main advantages of LAURDAN, is that its fluorescence photophysics has been extensively studied in lipid membranes for more

than 30 years (Bagatolli, 2013; Gunther et al., 2021; Parasassi, De Stasio, d'Ubaldo, & Gratton, 1990; Parasassi, De Stasio, Ravagnan, Rusch, & Gratton, 1991). We know that the LAURDAN emission spectrum is affected by the combined effect of membrane polarity, which is related to the apparent dielectric constant at the probe location in the membrane, and the dipolar relaxation process. Depending on the physical properties of the membrane, both the number of confined water molecules and their relaxation rates are modified (Gunther et al., 2021). For example, lipid bilayers in the liquid phase (L_α) are less packed, more hydrated and have a higher polarity compared to those in a gel (L_β) or liquid ordered (L_o) phase. Membranes in the L_α phase exhibit higher dipolar relaxation, because the water molecules are able to reorient around the LAURDAN moiety during its excited state; the dye spectrum is red-shifted. In contrast, membranes in the L_β or L_o phases are highly packed and dehydrated (low polarity), and the few water molecules present in the bilayer are unable to reorient while the dye is in the excited state; the LAURDAN spectrum is then blue-shifted. This general response is summarized in Fig. 1D, which shows that LAURDAN fluorescence displays a big spectral shift (~50 nm) between the liquid phase and the gel phases. It is important to emphasize that LAURDAN is sensitive to a wide range of intermediate membrane hydration states between these extremes (Golfetto, Hinde, & Gratton, 2015; Gratton & Digman, 2014; Malacrida et al., 2016; Mangiarotti & Bagatolli, 2021; Mangiarotti, Siri, et al., 2023), which are related to different degrees of lipid packing, as we will show in the next section. Considering all of the above, we will use the term "fluidity" throughout this chapter to refer to the ordering of the membrane headgroup-chain interface of a phospholipid bilayer.

1.2 Hyperspectral imaging and phasor analysis

Today, the capabilities of microscopes, such as spectral or lifetime resolution, not only enable us to acquire qualitative spatial information, but also to extract quantitative data from each pixel of an image (Malacrida, 2023). As shown in Fig. 2, akin to acquiring a spectrum in a fluorimeter, hyperspectral imaging involves capturing images at different wavelengths. Unlike "spectral", the term "hyperspectral" signifies that the measured spectral bands are narrow and contiguous, enabling high spectral resolution. The result is a stack of images, in which each pixel contains spectral information. While in the past extracting information from this method required specialized knowledge, the application of the phasor approach to the analysis of hyperspectral data has broadened

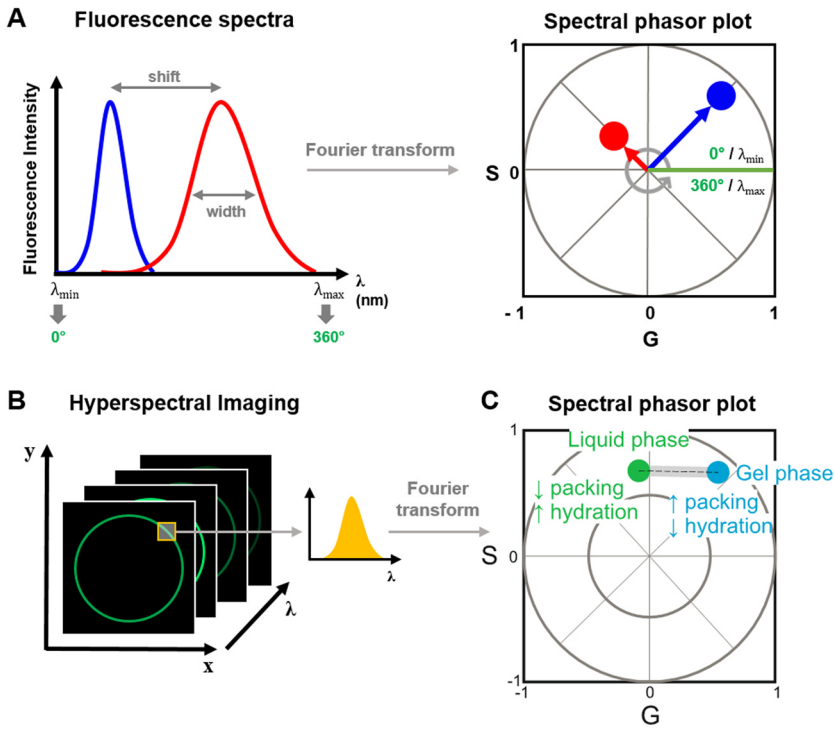

Fig. 2 (A) The spectral phasor transform converts the fluorescence spectra into vectors (phasors) in the Fourier space. In the spectral phasor plot, the wavelength increase is visualized counterclockwise (see gray arrow) beginning and ending in the green line at (1,0). Changes in the center of mass of the spectrum are visualized as changes in the angular position of the phasor; while the spectral width is related to the distance from the center of the plot (0,0). (B) Hyperspectral imaging consists of a xyλ stack generated by taking images at different emission wavelengths. In the final image stack, each pixel contains the full spectrum. (C) Sketch of a spectral phasor plot showing the trajectory for LAURDAN fluorescence in membranes. Due to the linear combination properties, spectra corresponding to different degrees of water penetration/membrane packing will fall within the linear trajectory between the two extremes for the liquid and the gel phases (Gratton & Digman, 2014; Gunther et al., 2021; Malacrida et al., 2021). Deviations from linearity would indicate the presence more components. *Panels (B) and (C) are adapted from Mangiarotti, A., Siri, M., Tam, N. W., Zhao, Z., Malacrida, L., & Dimova, R. (2023). Biomolecular condensates modulate membrane lipid packing and hydration. Nature Communications, 14(1), 6081.*

the use of this technique, as it is a model-free method that does not require prior knowledge of the spectral properties of the dyes in the sample (Malacrida, 2023; Malacrida, Ranjit, Jameson, & Gratton, 2021; Ranjit, Malacrida, Jameson, & Gratton, 2018). The first application of the phasor plot

was used to represent fluorescence lifetime imaging (FLIM) data (Digman, Caiolfa, Zamai, & Gratton, 2008; Hanley & Clayton, 2005; Redford & Clegg, 2005), and it was later applied to hyperspectral imaging (Fereidouni, Bader, & Gerritsen, 2012). The requirements for experimental setups to perform hyperspectral imaging are less demanding compared to FLIM (e.g., the latter requires the use of pulsed or modulated light sources and time-correlated single-photon counting systems). Because of this, and also due to their wider availability, we will focus on phasor analysis of hyperspectral imaging data.

In hyperspectral imaging, the phasor transformation, called spectral phasor, calculates the real (G) and imaginary (S) components of the spectral Fourier transform at each pixel. The Cartesian coordinates (G, S) of the spectral phasor plot are defined by the following expressions:

$$G = \frac{\int_{\lambda_{\min}}^{\lambda_{\max}} I(\lambda) \cos\left(\frac{2\pi n(\lambda - \lambda_i)}{\lambda_{\max} - \lambda_{\min}}\right) d\lambda}{\int_{\lambda_{\min}}^{\lambda_{\max}} I(\lambda)\, d\lambda} \tag{1}$$

$$S = \frac{\int_{\lambda_{\min}}^{\lambda_{\max}} I(\lambda) \sin\left(\frac{2\pi n(\lambda - \lambda_i)}{\lambda_{\max} - \lambda_{\min}}\right) d\lambda}{\int_{\lambda_{\min}}^{\lambda_{\max}} I(\lambda)\, d\lambda} \tag{2}$$

where, for a given pixel, $I(\lambda)$ represents the intensity as a function of wavelength, n is the harmonic number and λ_i is the initial wavelength. In this manner, each pixel in the image will be transformed into a vector in the Fourier space, called phasor. As we will discuss later, the definition of the range from $\lambda_{\min}$ to $\lambda_{\max}$ will determine the phasor position in the plot.

The spectral phasor position of a given pixel carries information about the spectral intensity profile of that pixel. As shown in Fig. 2A, the angular dependence carries information about the center of mass of the emission spectra, while the spectral width is reflected in the distance from the center. A key advantage of this approach is that it follows the rules of vector algebra, known as the linear combination property of phasors (Digman & Gratton, 2015; Torrado, Malacrida, & Ranjit, 2022). This means that for a pixel with two components (e.g. a mixture of two dyes or the same dye in two different environments), the phasor point will appear along a linear trajectory connecting the two pure components (see Fig. 2C). The fraction of each component is determined by the coefficients of the linear combination. If there are three components in a given pixel, the phasor position

will be inside a triangle whose vertices correspond to the pure components; this approach can be extended to any number of components and the corresponding polygons (Digman & Gratton, 2015; Torrado et al., 2022).

1.3 Spectral phasors vs generalized polarization

As explained in the previous sections, LAURDAN fluorescence in membranes produces different spectra depending on the degree of packing and hydration (Fig. 3A). One of the most popular approaches to analyze LAURDAN fluorescence in membranes, is to quantify the fluorescence at two fixed wavelengths, typically 440 nm and 490 nm corresponding to the emission maxima of the liquid and gel phases, respectively. From them, one can calculate the generalized polarization (GP) defined as (Parasassi et al., 1990):

$$GP = \frac{I_{440} - I_{490}}{I_{440} + I_{490}} \tag{3}$$

Here I_{440} and I_{490} are the fluorescence intensities measured at 440 nm and 490 nm, respectively. The GP function takes values between 1 and −1, where GP values of 0.5–0.6 generally correspond to bilayers in the gel phase state, and values near or below 0 correspond to liquid-disordered phases (Bagatolli, 2013), as shown in Fig. 3B. While this method has the advantage that it can be quickly implemented for cuvette or microscopy experiments, its main disadvantage is that it assumes a linear two-state model. This means that any component outside the linear GP range is not considered, and important information may be lost (Gunther et al., 2021; Malacrida, Gratton, & Jameson, 2015). In addition, because only two emission channels are being used for the GP determination, the sensitivity to spectral differences is reduced compared to the phasor approach, which uses the entire spectrum (Golfetto et al., 2015). While better spatial resolution has been achieved by using hyperspectral imaging to determine the GP values (Sezgin, Waithe, Bernardino de la Serna, & Eggeling, 2015), most of the spectral information is lost when the analysis is reduced to only two wavelength ranges (Gunther et al., 2021). It is also important to note that while GP is completely defined by one number, the spectral phasor is defined by two quantities (G and S) allowing for a more detailed description and interpretation of the underlying phenomena (Malacrida et al., 2015), as we will show in the next sections.

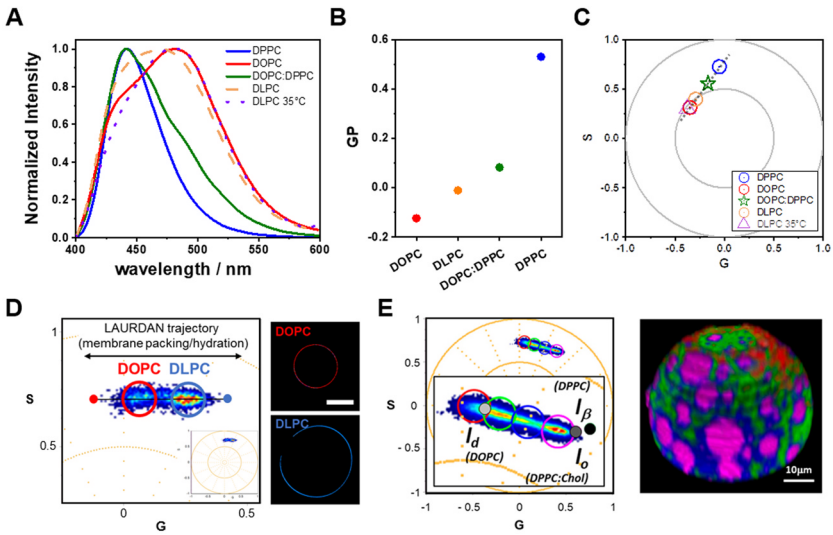

Fig. 3 (A) Normalized LAURDAN fluorescence spectra for multilamellar vesicles composed of DOPC, DLPC, DPPC, DPPC:DOPC 1:1 at 20 °C, and DLPC membranes at 35 °C (cuvette experiments). (B) LAURDAN GP for multilamellar vesicles of the indicated lipid compositions at 20 °C. (C) Spectral phasor plot for the spectra shown in (A), showing that the data arranges within a linear trajectory. The inset shows the complete graph. (D) LAURDAN-labeled DOPC and DLPC giant unilamellar vesicles display a linear trajectory in the phasor plot, corresponding to different hydration and packing states. The pixel clouds are colored from blue to red according to pixel density. By using circular cursors to select the pixel clouds in the phasor plot, the corresponding images are colored accordingly. The scale bar is 10 μm. (E) Spectral phasor plot of a GUV composed of DOPC:SM:cholesterol (1:1:1) labeled with LAURDAN. The black and gray dots indicate the phasors for gel (DPPC), liquid ordered (DPPC:Chol 70:30), and liquid disordered (DOPC) phases. The image shows a 3D projection of the GUV colored by using the cursor selection and their respective color scheme. *Panels A–C are adapted from Mangiarotti, A., & Bagatolli, L. A. (2021). Impact of macromolecular crowding on the mesomorphic behavior of lipid self-assemblies. Biochimica et Biophysica Acta (BBA) – Biomembranes, 1863(12), 183728; panel D was adapted from Mangiarotti, A., Siri, M., Tam, N. W., Zhao, Z., Malacrida, L., & Dimova, R. (2023). Biomolecular condensates modulate membrane lipid packing and hydration. Nature Communications, 14(1), 6081; and panel E is adapted from Gunther, G., Malacrida, L., Jameson, D. M., Gratton, E., & Sánchez, S. A. (2021). LAURDAN since Weber: The quest for visualizing membrane heterogeneity. Accounts of Chemical Research, 54(4), 976–987.*

1.4 Spectral phasor plot for LAURDAN fluorescence in model membranes

Analysis of the LAURDAN spectral phasor has proven to offer a versatile and precise tool for the interpretation of phenomena occurring at the membrane interface both in vitro (Gunther et al., 2021; Malacrida et al., 2015;

Mangiarotti & Bagatolli, 2021; Mangiarotti, Siri, et al., 2023) and in cells (Golfetto et al., 2015; Gunther et al., 2021; Malacrida et al., 2016; Vallmitjana, Lepanto, Irigoin, & Malacrida, 2023), providing a fingerprint of the molecular environment.

Due to the linear combination properties of the Fourier space, membranes containing LAURDAN and exhibiting different degrees of packing and hydration states will produce a linear trajectory in the spectral phasor plot (see Fig. 3C). The extremes of this linear trajectory correspond to the liquid and gel phases (Golfetto et al., 2015; Gratton & Digman, 2014; Gunther et al., 2021), as seen in Fig. 3C. It can be observed that, when moving from DPPC (L_β at 20 °C) to DOPC (L_α), the phasor for LAURDAN moves counter-clockwise due to the red shift of the center of mass, and closer to the radial center (0;0) due to the increase in the spectral width (Mangiarotti & Bagatolli, 2021). As expected, since the DOPC:DPPC mixture displays L_α/L_β phase coexistence, LAURDAN will emit from relaxed and unrelaxed states, and the phasor falls within the linear trajectory between the pure components. If the dynamics of water relaxation at the membrane interface is modified in any way, the LAURDAN spectrum will be modified and the phasor will consequently change its position. This is illustrated for DLPC in Fig. 3C: at 35 °C DLPC shows higher fluidity and dipolar relaxation than at 20 °C, and this can be easily visualized by the change in the position of the phasor in the plot (Mangiarotti & Bagatolli, 2021). It is important to note that, even though DOPC and DLPC at 20 °C and DLPC at 35 °C are all membranes in the liquid phase, they exhibit differences in the degree of packing and dipolar relaxation, and LAURDAN fluorescence can distinguish between these subtle changes. Because we are evaluating changes in the lipid packing and hydration, all the data points fall within the same linear trajectory, and any deviation from this trajectory would indicate the presence of more than two components. This situation can occur if LAURDAN is emitting from an environment different from a membrane, e.g. if the probe binds to a protein or partitions to a protein-rich phase (Mangiarotti, Siri, et al., 2023), or from a structure different from a bilayer, like other mesomorphic phases (Mangiarotti & Bagatolli, 2021). Thus, phasor changes along the linear combination trajectory for LAURDAN fluorescence correspond to a measure of water penetration in the lipid bilayer, providing an empirical measure of membrane fluidity (Gratton & Digman, 2014). While the phasor approach for FLIM allows separating the polarity changes from the dipolar relaxations (Golfetto, Hinde, & Gratton, 2013; Malacrida et al., 2021; Mangiarotti & Bagatolli, 2021; Mangiarotti, Siri, et al., 2023), with the spectral phasor approach both

variables are measured together (Gunther et al., 2021; Mangiarotti & Bagatolli, 2021; Mangiarotti, Siri, et al., 2023). For this reason, we will use the term fluidity to refer to changes in both, polarity and dipolar relaxation.

While in cuvette experiments, each spectrum is represented by a point in the phasor plot (Fig. 3C), in hyperspectral imaging, since each pixel contains spectral information, the transformation results in a pixel cloud, as can be seen in Fig. 3D for DOPC and DLPC giant vesicles. In this example, as well as in Fig. 3E, it can be seen that the data points themselves are arranged on a linear trajectory, corresponding to a linear combination between two surrounding environments for LAURDAN. Note that it is not necessary to know the extreme points of the trajectory. Fig. 3E shows the case of an equimolar complex mixture composed of DOPC, sphingomyelin (SM) and cholesterol, and in this case the linear trajectory is delimited by the L_α and L_o phases.

One of the most outstanding and useful features of the phasor approach is the reciprocity principle (Malacrida et al., 2021; Ranjit et al., 2018), by which cursors (or a continuous color scheme) can be used to select a region of pixels in the phasor plot and then the corresponding pixels in the images are colored accordingly, as shown in Fig. 3D and E. The reciprocity principle allows for an immediate qualitative spatial visualization of the changes taking place.

Note that the phasor position changes depending on the selected detection range (see Eqs. 1 and 2). While in Fig. 3C the detection range was 400–600 nm, for Fig. 3D and E the range used was 416–728 nm as we will discuss below. A wider detection range provides increased resolution.

2. Preparing giant unilamellar vesicles for hyperspectral imaging measurements

We will focus on the application of spectral phasor analysis for a model membrane system, namely giant unilamellar vesicles (GUVs) (Dimova & Marques, 2019). However, as mentioned above, this method can be extended to various other membrane model systems, and cells (Golfetto et al., 2015; Gratton & Digman, 2014). While there are several preparation methods that can be used to generate GUVs (see e.g. detailed protocols in (Dimova & Marques, 2019)), here we will use the electroformation method, developed by Angelova and Dimitrov (1986). The complete procedure as described below takes about 2.5–3 h and it is

recommended to use freshly prepared vesicles for the experiments, to avoid issues with lipid oxidation and dye bleaching.

After the GUVs are prepared, a key aspect of sample preparation for hyperspectral imaging consists in preventing their movement during image acquisition (e.g. avoiding vesicle drift). In this regard, there are several protocols for GUV immobilization, such as employing density gradients across the membrane using sugars, GUV adhesion to the substrate using biotinylated lipids and glass support coated with streptavidin (Dimova & Marques, 2019), or immobilization in agarose gels (Lira, Steinkühler, Knorr, Dimova, & Riske, 2016). Here, we use the sucrose-glucose density gradient, which is a simple method that allows GUVs to sediment to the bottom of the chamber and to remain stable against drift.

2.1 Equipment

Glass vials (0.5-1 mL)
Hamilton syringe (10 μL)
Osmometer
Function generator
Indium tin oxide coated glass slides (ITOs). Typical dimensions are 5 cm × 5 cm with a resistivity of 30–60 Ohm/sq.
Copper tape
Teflon spacer (2 mm thickness)
Multimeter
Lab oven (50–60 °C)
Binder clips
Vacuum chamber

2.2 Buffers and reagents

Sucrose
Glucose
Chloroform
Lipids

2.3 Procedure

1. Using the multimeter determine the conductive side of the ITO plates, probe that their resistance is correct and attach a copper tape to that side, as shown in Fig. 4A.
2. Prepare stocks of the pure lipids in chloroform and the corresponding lipid mixtures to a final concentration of approximately 4 mM.

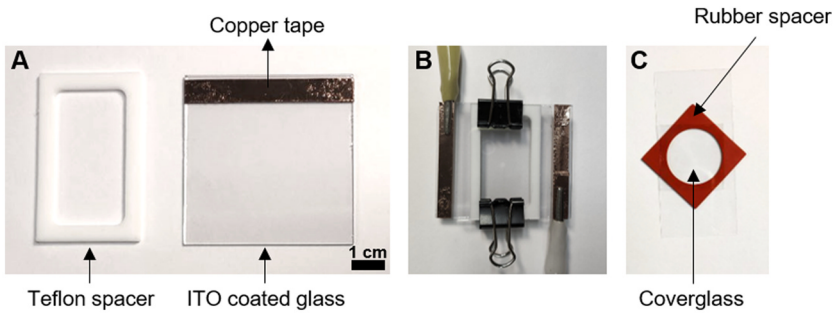

Fig. 4 (A) ITO-coated glass for vesicle electroformation and Teflon spacer for chamber assembly. (B) Assembled chamber for GUV electroformation. The Teflon spacer is sandwiched between the conductive sides of the ITO-coated glasses and held together by binder clips. The copper tapes are clamped by the connectors to the AC filed generator (C). The chamber for confocal microscopy observation is constructed by using a 0.17 mm thickness coverglass, a rubber spacer, and a square coverglass to seal it and prevent evaporation and drift.

3. Using a Hamilton syringe, evenly spread 4 μL of the desired lipid mixture at the center of each ITO glass using the tip of the syringe, and assemble the chamber as shown in Fig. 4B.
4. Place the ITOs in a vacuum chamber for 1 h to remove traces of chloroform.
5. Prepare sucrose and glucose solutions (e.g. 100 mM) matching their osmolarities (using an osmometer).
6. Fill the chamber with the sucrose solution, and close it with binder clips preventing the formation of air bubbles (Fig. 4B).
7. Connect the chamber to the function generator, and apply a sinusoidal voltage (1.5 V) at a frequency of 10 Hz for 1 h. This is just an example of parameters that can be applied to sucrose solutions, and different electroformation protocols must be used depending on the buffer salinity (Méléard, Bagatolli, & Pott, 2009). When using cholesterol or high melting temperature lipids such as DPPC or SM, electroformation must be performed above the melting temperature of the mixture. In this case, the chamber should be placed in the oven at the appropriate temperature ($T_{electroformation} > T_{melting}$) during electroformation.
8. After electroformation, carefully extract the chamber content and store it in a glass vial preventing light exposure to avoid dye bleaching (e.g. cover with aluminum foil or use brown tinted vials).

2.4 Notes

The GUVs can be stored in sucrose, or directly diluted in glucose in a 1:1 vol ratio.

3. Measuring hyperspectral images of giant unilamellar vesicles

Either a 405 nm laser or a multi-photon laser (two-photon excitation at 720–780 nm) can be used for LAURDAN excitation. The advantage of using two-photon excitation is that dye photobleaching is minimized because the excitation volume is significantly reduced compared to that in confocal microscopy. However, 405 nm continuous-wave excitation can also be used, provided that photobleaching does not interfere with the measurements. In this case, a good alternative is to use LAURDAN derivatives with higher photostability, such as C-Laurdan (Kim et al., 2007). Other solvatochromic probes with excitation at higher wavelengths such as Nile Red and derivatives, also show a large spectral shift and higher photostability (Ragaller et al., 2022). For example, Nile Red hyperspectral imaging combined with phasor analysis showed a high sensitivity to changes in membrane order (Sameni, Malacrida, Tan, & Digman, 2018).

3.1 Equipment

Confocal microscope with spectral detection (e.g. Zeiss LSM 780/880/980 have 32 channels array detectors; Leica TCS SP5/SP8 have single PMTs or hybrid detectors).
405 nm laser or multi-photon excitation at 720–780 nm (for LAURDAN)
Objective with high numerical aperture.
Coverglass
Rubber spacer

3.2 Buffers and reagents

Bovine serum albumin fatty acid free (BSA)
Deionized water

3.3 Procedure

1. Passivate the coverglass surface by incubation with a 2 mg/mL BSA solution (approx. 10 min). After drying, rinse the glass with deionized

water to remove excess protein. This will prevent GUV from collapsing and spreading over the glass surface.
2. Assemble a chamber with a coverglass and the rubber spacer as shown in Fig. 4C.
3. Place an aliquot of the sample (50–100 μL) on the coverglass and seal to prevent evaporation and drift (Fig. 4C). After preparation, the GUV sample should be diluted in glucose, at least at 1:1 ratio, to ensure that the GUVs sediment to the bottom of the chamber, and to prevent them from floating and moving.
4. Use a high numerical aperture objective such as 63×, NA1.2 (water immersion) or 40×, NA1.4 (oil immersion).
5. Adjust laser power and gain until the image is clear enough without saturation.
6. Set the image size to 512 × 512 pixels or 256 × 256 pixels.
7. Set the scan speed to 200–400 Hz.
8. Set the spectral acquisition mode (e.g. in Leica SP5/SP8 it is called xyλ).
9. Set the detection range between 416 and 728 nm.
10. Set the bandwidth to 9.75 nm to obtain 32 channels.
11. Zoom-in until the pixel size is about 70 nm.
12. Acquire the images. Each file will be a stack of 32 images.

3.4 Notes

1. The selection of the detection range is of key importance. In general, commercial detectors only allow the collection of a portion of the emission spectrum, but one should try to obtain the whole spectrum or as large portion of it as possible. In this manner, by detecting between 416 and 728 nm we obtain most of the LAURDAN spectrum in different environments (see Fig. 3A for reference). When using different dyes, the range should be adjusted to cover as much of the emission spectrum as possible. If the spectrum is truncated, the transformation will result in a breakdown of linearity (Malacrida et al., 2015; Torrado et al., 2022). While having a few channels will decrease sensitivity, having too many channels will contribute to a decrease in signal-to-noise ratio (Torrado et al., 2022).
2. The suggested scan speed and the pixel size are based on empirical optimizations (Golfetto et al., 2015; Gratton & Digman, 2014; Malacrida et al., 2016; Mangiarotti, Siri, et al., 2023), and respond to a trade-off between the acquisition time (e.g. if it is too long, it can lead to photobleaching) and the number of collected photons, which determines the signal-to-noise ratio.

3. In general, each image stack should take about 1 min. To increase the speed, the bidirectional mode can be used.
4. It is important to avoid pixel saturation. For this purpose, the laser power and the gain should be adjusted so that no channel is saturated. Most microscope's software allow to change the visualization mode to a high-low function that allows to check the over/under exposure.
5. Once the correct parameters have been found and set, they should be kept fixed for all experiments in order to be able to compare them. In particular, changing the detection range will move the phasor position, as mentioned before.
6. If there is some movement of the vesicles during acquisition, such as lateral movement, and the sample does not move out of the field of view, it is possible to solve this problem by aligning the images of the stack before transformation. This can be done by using some frame matching and alignment plugins for ImageJ, such as the one developed by Qinzong Tseng (available at https://sites.imagej.net/Template_Matching/).

4. Using phasor analysis for hyperspectral imaging

A number of free software and scripts are available to perform the phasor transformation of the images and to visualize the phasor plots for analysis. The software "SimFCS" (http://www.lfd.uci.edu/globals/) was developed by the Laboratory of Fluorescence Dynamics (LFD) at the University of California, Irvine. A very detailed protocol for the use of SimFCS for the analysis of FLIM images has been published (Ranjit et al., 2018), and in general, the same principles and steps apply to spectral phasor analysis. Another available software is "PhasorM" developed by Maulucci's group, which also provided a detailed protocol for its use (Di Giacinto, De Angelis, De Spirito, & Maulucci, 2018). The most recent development is the Python-based open library "PhasorPy" created by Malacrida's group in cooperation with the LFD (Malacrida, 2023), available in the GitHub repository (https://github.com/ubaimaging/PhasorPy.git).

Since detailed protocols for phasor transformation are available (Di Giacinto et al., 2018; Ranjit et al., 2018), in this section we will focus on some examples and provide suggestions for proper image processing and analysis. The first step after correct image acquisition is to ensure that we analyze the information of interest. To do this, it is necessary to select the important information and discard the rest. This can be done in different ways, for example by applying

masks or thresholds in image processing softwares such as ImageJ, or by directly selecting the pixels of interest from the histogram in SimFCS, as shown in Fig. 5. Fig. 5A shows a hyperspectral image (xyλ stack) of a DOPC GUV containing 0.5 mol% LAURDAN. From the histogram shown in Fig. 5B, the low intensity pixels corresponding to the background (Fig. 5C and blue region in Fig. 5B) and the saturated pixels can be discarded, and we can keep only the

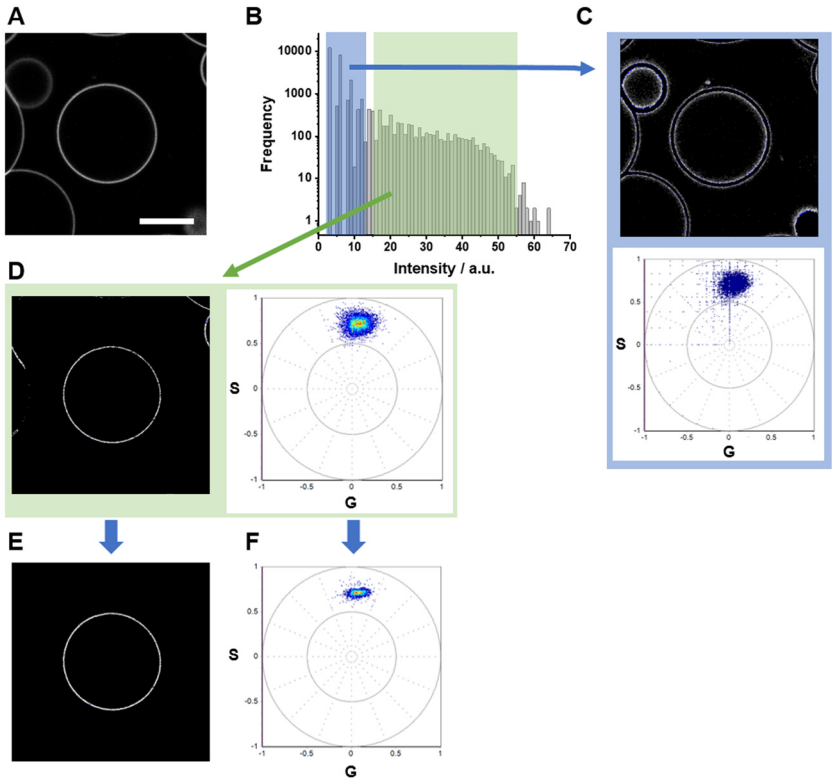

Fig. 5 Image processing and masking. (A) Sum of all 32 slices from the hyperspectral stack. Scale bar: 10 μm. (B) Intensity histogram over all pixels in the image shown in a. Blue and green shading show regions of interest processed in (C) and (D), respectively. (C) The image shows the selection of the lower intensity pixels in B, and below the corresponding points in the phasor plot. (D) The intermediate intensity pixels contain the information of interest as shown in the image and phasor plot on the right. (E) Further masking (e.g. by selecting pixels), allow us to only analyze the pixels of interest, in this case we only kept the vesicle in the middle of the image. (F) By applying a median filter in SimFCS to the G and S coordinates, the variance of the phasor location is reduced while keeping the spatial resolution of the original image (Digman & Gratton, 2015; Ranjit et al., 2018).

pixels of interest that have intermediate intensities (Fig. 5D). Fig. 5E shows that by using a mask we could keep only the vesicle in the center of the image. Finally, with SimFCS it is possible to apply a median filter, which reduces the variance of the phasor position at each pixel while maintaining the spatial resolution of the original image. This filtering procedure is explained in detail in (Digman & Gratton, 2015; Ranjit et al., 2018) for FLIM, but the same applies for hyperspectral imaging.

Once the images have been masked and filtered, the phasor plot properties such as linear combinations and reciprocity (shown in Fig. 3) can be used to analyze the data. Fig. 6 shows an example of the use of phasors to assess membrane order. In this system, the influence of protein condensates on membrane order is evaluated. In this example, we employed glycinin condensates in contact with the membrane. Glycinin is a soybean protein that phase separates in the presence of sodium chloride (Chen, Zhao, Wang, & Dimova, 2020), and exhibits salt-dependent material properties (Mangiarotti, Siri, et al., 2023). In the presence of GUVs, glycinin condensates can undergo two wetting transitions from dewetting to partial wetting, and from partial wetting to complete wetting (Mangiarotti, Chen, Zhao, Lipowsky, & Dimova, 2023). Fig. 6A shows examples of DOPC GUVs in contact with glycinin condensates at different concentrations of sodium chloride. It can be seen that increasing the salt concentration leads to an increased membrane-condensate interaction (higher degree of wetting), as evidenced by condensate spreading and mutual remodeling of the membrane and condensate. If the GUVs are labeled with LAURDAN, and the glycinin condensates are unlabeled, it is possible to analyze the effect of the condensates on the membrane order. Fig. 6B shows an example of a LAURDAN-labeled DOPC GUV in contact with an unlabeled condensate. Using hyperspectral imaging and phasor analysis, it is possible to distinguish different degrees of membrane packing between the segment of the membrane wetted by the condensate and the bare (condensate-free) membrane. The inset of the graph in Fig. 6B shows the phasor plot, and it can be seen that the data are organized along a linear trajectory. This indicates that the observed distribution is a combination of two state components, in the case of LAURDAN between a relaxed and non-relaxed environment. Using the reciprocity principle, pixels in the phasor plot can be selected with cursors and the corresponding pixels in the image are colored accordingly. In this way, it is easy to see that the wetted segment of the membrane has increased packing compared to the bare membrane. The linear combination properties of the phasor space

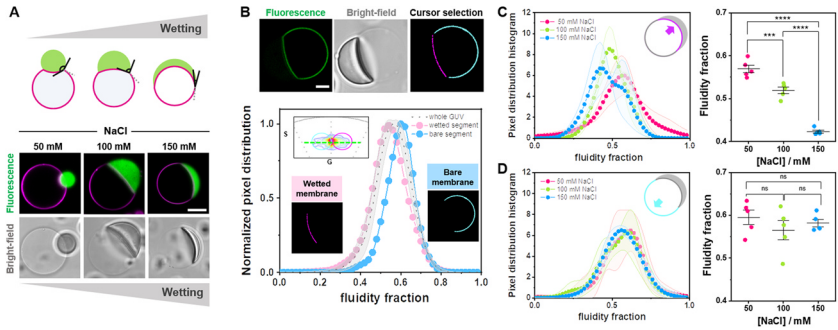

Fig. 6 Spectral phasor analysis of GUVs in contact with glycinin condensates. (A) Biomolecular condensates can wet membranes (Li, Lipowsky, & Dimova, 2008; Mangiarotti, Chen, et al., 2023), and the increase in wetting can be observed as an increase in the spreading of the droplet over the membrane, as well as a decrease in the contact angle as illustrated in the sketch (upper panel). Examples of partial wetting of DOPC GUVs by glycinin condensates at the indicated NaCl concentrations (bottom panel). Scale bar: 10 μm. (B–D) DOPC GUVs labeled with 0.5 mol% LAURDAN (in contact with unlabeled condensates. Using LAURDAN fluorescence spectral phasor analysis, the vesicle can be segmented and the contributions of the membrane in contact with the condensate and the bare membrane can be separated. (B) Example analysis for a single DOPC GUV labeled with 0.5% LAURDAN (green) in contact with an unlabeled condensate at 100 mM NaCl. The cursor-colored segments and the corresponding histograms are shown in the bottom panel. The part of the membrane in contact with the condensate is more packed (lower fluidity fraction) than the bare membrane. Distributions were normalized for clarity. Scale bar: 10 μm. (C and D) Histograms of the pixel distribution (left panel), and center of mass of the distributions (right panel) for the membrane segment in contact with the condensate (C) and for the bare membrane segment (D), at the indicated NaCl concentrations. The sketches indicate the part of the membrane being analyzed. The statistical analysis was performed with One-way ANOVA and Tukey post-test analysis ($p < 0.0001$, **** | $p < 0.001$, *** | ns = non-significant). *Adapted from Mangiarotti, A., Siri, M., Tam, N. W., Zhao, Z., Malacrida, L., & Dimova, R. (2023). Biomolecular condensates modulate membrane lipid packing and hydration. Nature Communications, 14(1), 6081.*

allow quantification and statistical analysis of the data. In this case, the extremes of the linear trajectory can be defined as the corresponding phasor positions for gel and liquid phases, for example, or can be arbitrarily defined. The two-component analysis provides the pixel distribution along the defined trajectory, which in this case corresponds to the fluidity fraction (packing degree). In Fig. 6B it can be seen that at the single vesicle level the bare membrane has a higher fluidity fraction than the wetted membrane. Then, by analyzing only the wetted segments of the membrane when interacting with condensates at different salinities, it can be seen that

increasing the sodium chloride concentration results in a decreased fluidity fraction (Fig. 6C). A useful way to statistically analyze the differences between the histograms is to calculate and compare the center of mass of each distribution (Fig. 6C and D, right panels). The center of mass can be calculated as:

$$CM = \frac{\sum_{i=0}^{i=1} F_i \, i}{\sum_{i=0}^{i=1} F_i} \tag{4}$$

where F_i is the fluidity fraction. Data can be compared and analyzed using statistical tests such as t-test or one-way ANOVA.

Analysis of the bare membrane segment shows that there are no significant differences in membrane packing at different salinities, as shown in Fig. 6D.

Note that if, for example, there was certain LAURDAN partitioning to the condensate, or the condensate showed autofluorescence, this would immediately show up in the phasor plot as a third component and a deviation from linearity (Mangiarotti, Siri, et al., 2023). This feature is a clear advantage over the GP analysis which only considers a two-state model, and would not distinguish such cases (Malacrida et al., 2015).

This analysis helped to uncover a general mechanism for condensates interacting with membranes (Mangiarotti, Siri, et al., 2023). Note that in this case we distinguish lateral heterogeneities in single-component membranes, highlighting the sensitivity of the phasor approach to evaluate small changes in membrane properties (Mangiarotti, Siri, et al., 2023).

Spectral phasor analysis has primarily been used to evaluate membrane packing and hydration in cells (Golfetto et al., 2015; Malacrida et al., 2016; Malacrida, Jameson, & Gratton, 2017; Sameni et al., 2018; Vallmitjana et al., 2023), but here we have demonstrated that it is a useful and versatile approach that can also be used to assess lateral heterogeneity in model membranes.

5. Summary and conclusions

Hyperspectral imaging combined with phasor analysis is a powerful tool that can be implemented in most laboratories equipped with a microscope with spectral detection. The phasor approach has many advantages because it is a fit-free graphical method that allows spectral changes to be understood by visual inspection without a priori knowledge

of the photophysics of the dye. In addition, the phasor space allows easy quantification of the fraction of multiple components using the linear combination rules. The high sensitivity of the method allows the measurement of small changes in membrane lipid packing (Mangiarotti, Siri, et al., 2023). This is a very useful tool for determining changes in membrane phase state in response to various stimuli such as osmotic pressure, interaction with peptides, proteins or other macromolecules, and wetting by soft materials such as the protein condensates shown here.

6. Connections

As mentioned above, the spectral phasor approach can be applied to different model systems and also to more complex systems, like cellular membranes. In this context, the spectral phasor approach could contribute to the characterization of a polymer-lipid hybrid system as described in the chapter by Cecilia Leal. Since the phasor method provides a fingerprint for the fluorescence of the dye in a given environment, it is possible to compare membranes with pure lipids with those containing polymers and also to test how the lipid packing and hydration change with different amounts of polymer/lipid species. The same is true for the pore-spanning membranes presented in Claudia Steinem's chapter. In addition, as we have shown, the phasor approach is very useful to measure membrane changes due to the interaction with proteins and condensates. It could be used to characterize changes in the multi-bilayer system introduced in the chapter of Kandice Levental, and on supported membranes such as those the described in the chapter by Karthik Narayan et al. Finally, other cues that change membrane properties, such as hydrostatic pressure, as introduced in the chapter by Nicholas Brooks, could be studied using the phasor approach for a dynamic visualization of the changes taking place at the membrane.

References

Angelova, M. I., & Dimitrov, D. S. (1986). Liposome electroformation. *Faraday Discussions, 81*, 303–311.

Bagatolli, L. A. (2013). LAURDAN fluorescence properties in membranes: A journey from the fluorometer to the microscope. In Y. Mély, & G. Duportail (Eds.). *Fluorescent methods to study biological membranes* (pp. 3–35). Berlin, Heidelberg: Springer Berlin Heidelberg.

Chen, N., Zhao, Z., Wang, Y., & Dimova, R. (2020). Resolving the mechanisms of soy glycinin self-coacervation and hollow-condensate formation. *ACS Macro Letters, 9*(12), 1844–1852.

Di Giacinto, F., De Angelis, C., De Spirito, M., & Maulucci, G. (2018). Quantitative imaging of membrane micropolarity in living cells and tissues by spectral phasors analysis. *MethodsX, 5*, 1399–1412.

Digman, M. A., Caiolfa, V. R., Zamai, M., & Gratton, E. (2008). The phasor approach to fluorescence lifetime imaging analysis. *Biophysical Journal, 94*(2), L14–L16.

Digman, M. A., & Gratton, E. (2015). The phasor approach to fluorescence lifetime imaging: Exploiting phasor linear properties. In L. Marcu, P. M. W. French, & D. S. Elson (Eds.). *Fluorescence lifetime spectroscopy and imaging, principles and applications in biomedical diagnostics* (pp. 570). CRC Press.

Dimova, R., & Marques, C. (2019). *The giant vesicle book*. Boca Raton, FL: Taylor & Francis Group, LLC.

Fereidouni, F., Bader, A. N., & Gerritsen, H. C. (2012). Spectral phasor analysis allows rapid and reliable unmixing of fluorescence microscopy spectral images. *Optics Express, 20*(12), 12729–12741.

Golfetto, O., Hinde, E., & Gratton, E. (2013). Laurdan fluorescence lifetime discriminates cholesterol content from changes in fluidity in living cell membranes. *Biophysical Journal, 104*(6), 1238–1247.

Golfetto, O., Hinde, E., & Gratton, E. (2015). The laurdan spectral phasor method to explore membrane micro-heterogeneity and lipid domains in live cells. In D. M. Owen (Ed.). *Methods in membrane lipids* (pp. 273–290). New York, NY: Springer New York.

Gratton, E., & Digman, M. A. (2014). Laurdan identifies different lipid membranes in eukaryotic cells. In A. Cambi, & D. S. Lidke (Eds.). *Cell membrane nanodomains: From biochemistry to nanoscopy* (pp. 510). CRC Press.

Gunther, G., Malacrida, L., Jameson, D. M., Gratton, E., & Sánchez, S. A. (2021). LAURDAN since Weber: The quest for visualizing membrane heterogeneity. *Accounts of Chemical Research, 54*(4), 976–987.

Hanley, Q. S., & Clayton, A. H. A. (2005). AB-plot assisted determination of fluorophore mixtures in a fluorescence lifetime microscope using spectra or quenchers. *Journal of Microscopy, 218*(1), 62–67.

Jurkiewicz, P., Olżyńska, A., Langner, M., & Hof, M. (2006). Headgroup hydration and mobility of DOTAP/DOPC bilayers: A fluorescence solvent relaxation study. *Langmuir: The ACS Journal of Surfaces and Colloids, 22*(21), 8741–8749.

Kim, H. M., Choo, H.-J., Jung, S.-Y., Ko, Y.-G., Park, W.-H., Jeon, S.-J., et al. (2007). A two-photon fluorescent probe for lipid raft imaging: C-Laurdan. *Chembiochem: A European Journal of Chemical Biology, 8*(5), 553–559.

Klymchenko, A. S. (2023). Fluorescent probes for lipid membranes: From the cell surface to organelles. *Accounts of Chemical Research, 56*(1), 1–12.

Leung, S. S. W., Brewer, J., Bagatolli, L. A., & Thewalt, J. L. (2019). Measuring molecular order for lipid membrane phase studies: Linear relationship between Laurdan generalized polarization and deuterium NMR order parameter. *Biochimica et Biophysica Acta (BBA) – Biomembranes, 1861*(12), 183053.

Li, Y., Lipowsky, R., & Dimova, R. (2008). Transition from complete to partial wetting within membrane compartments. *Journal of the American Chemical Society, 130*(37), 12252–12253.

Lira, R. B., Steinkühler, J., Knorr, R. L., Dimova, R., & Riske, K. A. (2016). Posing for a picture: Vesicle immobilization in agarose gel. *Scientific Reports, 6*, 25254.

Malacrida, L. (2023). Phasor plots and the future of spectral and lifetime imaging. *Nature Methods, 20*(7), 965–967.

Malacrida, L., Astrada, S., Briva, A., Bollati-Fogolín, M., Gratton, E., & Bagatolli, L. A. (2016). Spectral phasor analysis of LAURDAN fluorescence in live A549 lung cells to study the hydration and time evolution of intracellular lamellar body-like structures. *Biochimica et Biophysica Acta (BBA) – Biomembranes, 1858*(11), 2625–2635.

Malacrida, L., Gratton, E., & Jameson, D. M. (2015). Model-free methods to study membrane environmental probes: A comparison of the spectral phasor and generalized polarization approaches. *Methods and Applications in Fluorescence, 3*(4), 047001.

Malacrida, L., Jameson, D. M., & Gratton, E. (2017). A multidimensional phasor approach reveals LAURDAN photophysics in NIH-3T3 cell membranes. *Scientific Reports, 7*(1), 9215.

Malacrida, L., Ranjit, S., Jameson, D. M., & Gratton, E. (2021). The phasor plot: A universal circle to advance fluorescence lifetime analysis and interpretation. *Annual Review of Biophysics, 50*(1), 575–593.

Mangiarotti, A., & Bagatolli, L. A. (2021). Impact of macromolecular crowding on the mesomorphic behavior of lipid self-assemblies. *Biochimica et Biophysica Acta (BBA) – Biomembranes, 1863*(12), 183728.

Mangiarotti, A., Chen, N., Zhao, Z., Lipowsky, R., & Dimova, R. (2023). Wetting and complex remodeling of membranes by biomolecular condensates. *Nature Communications, 14*(1), 2809.

Mangiarotti, A., Siri, M., Tam, N. W., Zhao, Z., Malacrida, L., & Dimova, R. (2023). Biomolecular condensates modulate membrane lipid packing and hydration. *Nature Communications, 14*(1), 6081.

Méléard, P., Bagatolli, L. A., & Pott, T. (2009). *Giant unilamellar vesicle electroformation: From lipid mixtures to native membranes under physiological conditions. Methods in Enzymology*, *465*, Academic Press161–176.

Parasassi, T., De Stasio, G., d'Ubaldo, A., & Gratton, E. (1990). Phase fluctuation in phospholipid membranes revealed by Laurdan fluorescence. *Biophysical Journal, 57*(6), 1179–1186.

Parasassi, T., De Stasio, G., Ravagnan, G., Rusch, R. M., & Gratton, E. (1991). Quantitation of lipid phases in phospholipid vesicles by the generalized polarization of Laurdan fluorescence. *Biophysical Journal, 60*(1), 179–189.

Ragaller, F., Andronico, L., Sykora, J., Kulig, W., Rog, T., Urem, Y. B., et al. (2022). Dissecting the mechanisms of environment sensitivity of smart probes for quantitative assessment of membrane properties. *Open Biology, 12*(9), 220175.

Ranjit, S., Malacrida, L., Jameson, D. M., & Gratton, E. (2018). Fit-free analysis of fluorescence lifetime imaging data using the phasor approach. *Nature Protocols, 13*(9), 1979–2004.

Redford, G. I., & Clegg, R. M. (2005). Polar plot representation for frequency-domain analysis of fluorescence lifetimes. *Journal of Fluorescence, 15*(5), 805–815.

Sameni, S., Malacrida, L., Tan, Z., & Digman, M. A. (2018). Alteration in fluidity of cell plasma membrane in huntington disease revealed by spectral phasor analysis. *Scientific Reports, 8*(1), 734.

Sanchez, S. A., Tricerri, M. A., & Gratton, E. (2012). Laurdan generalized polarization fluctuations measures membrane packing micro-heterogeneity in vivo. *Proceedings of the National Academy of Sciences, 109*(19), 7314–7319.

Sezgin, E., Waithe, D., Bernardino de la Serna, J., & Eggeling, C. (2015). Spectral imaging to measure heterogeneity in membrane lipid packing. *Chemphyschem: A European Journal of Chemical Physics and Physical Chemistry, 16*(7), 1387–1394.

Torrado, B., Malacrida, L., & Ranjit, S. (2022). Linear combination properties of the phasor space in fluorescence imaging. *Sensors, 22*(3), https://doi.org/10.3390/s22030999.

Vallmitjana, A., Lepanto, P., Irigoin, F., & Malacrida, L. (2023). Phasor-based multi-harmonic unmixing for in-vivo hyperspectral imaging. *Methods and Applications in Fluorescence, 11*(1), 014001.

Weber, G., & Farris, F. J. (1979). Synthesis and spectral properties of a hydrophobic fluorescent probe: 6-Propionyl-2-(dimethylamino)naphthalene. *Biochemistry, 18*(14), 3075–3078.